Numerical study of the complete operating map of ejectors in Ultra High Bypass Ratio engine bleed systems

Jagadish Babu Vemula, Matthieu Duponcheel, Yann Bartosiewicz

Université catholique de Louvain (UCLouvain),
Institute of Mechanics, Materials, and Civil engineering (iMMC),
Louvain-la-Neuve, Belgium, B-1348.

Abstract

New bleed systems are needed for the aircraft based on Ultra High Bypass Ratio (UHBR) engines to improve its overall efficiency, and one of the solutions is to utilize air ejectors to optimize the bleed air system. The present numerical study investigates the behavior of the ejector via entrainment ratio, limiting pressure ratios, and the performance dependency on different operating regimes. Within each regime, the ejector's performance depends on the operating conditions, such as total pressures and temperatures given at inlets and outlets. To explore the whole operating map at a fixed temperature ratio, the numerical simulations are classified according to the primary flow and the secondary flow. Combining these two classifications allows us completely to characterize the flow in the ejector. Furthermore, variation in the inlet temperatures show a prominent effect on the mass flow rates and entrainment ratio.

Keywords Mass flow rates, entrainment ratio, pressure ratio, temperature ratio.

1 Introduction

An ejector is a simple device that uses the energy within a high-pressure primary flow to entrain and compress a low-pressure secondary flow to an intermediate back pressure. Due to their simple design, with no moving parts and no direct mechanical power input (See in Fig. 1 (left)), the ejectors are widely used in various sectors, like energy [Kulkarni et al.(2022), Konstantinos (2021), Sagar et al.(2021)], refrigeration [Besagni et al.(2016), Qudama et al.(2022), Yann et al.(2006)], and aerospace applications [Vincent et al.(2012)]. Within the Clean-Sky2 - Engine bleed JEt pumps continuous behaviour MODelization (EJEMOD) project [CleanSky2 (2021)], the current work focuses on applying an air ejector for UHBR aircraft engines. Here, the ejector uses the engine bleed air as a primary motive stream to entrain and mix with a lower pressure secondary stream. However, the ejector does not necessarily work in normal conditions for the UHBR application, justifying an in depth analysis through the entire possible range of operation, including abnormal conditions. Thus, the present numerical analysis aims to investigate the ejector performance for the entire possible range of operation. Further, the present CFD results assist in developing an accurate and robust 0D model to model the ejector behavior [EUCASS (2022)]. The typical layout of a supersonic ejector is shown on Fig. 1 (left). Fig. 1 (right) depicts the classical characteristic curve where the ejector operates in critical (on-design) mode, performing with maximum entrainment ratio. In the subcritical (off-design) mode, the entrainment ratio is between the maximum and zero. Finally, in the abnormal (back-flow)

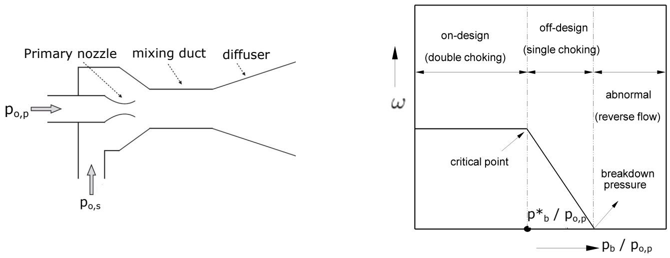

Figure 1: Typical layout of a supersonic ejector (left) and its classical characteristic curve (right)

mode, it is less than or equal to zero. Here, the entrainment ratio (w) is the ratio of secondary mass flow rate ($\dot{m}_s$) and primary mass flow rate ($\dot{m}_p$).

2 Numerical methodology

The corresponding 2D-axisymmetric computational domain of the ejector used for the Reynolds averaged Navier-Stokes equations (RANS) simulations is shown in Fig. 2 (left). The steady-state RANS simulations are performed on the near wall-refined mesh (grid convergence study is shown in Fig. 2 (right)) using the Ansys Fluent (2020 R1) - pressure based coupled solver with the ideal gas assumptions. The mesh refinement in the vertical direction ensures that the center of the cell adjacent to the wall is always at $y^+ < 1$, as shown in Figure 2. The value of Grid Convergence Index (GCI) from coarser to finer grid was found to be decreasing as the grid was refined. The finer grid was relevant to be applied for all the simulations as the value of GCI is approximately one. Regarding the type of boundary conditions, pressure-inlet at the inlet sections and pressure-outlet at the outlet section are used. The total pressure is imposed at the primary nozzle ($p_{o,p}$) and secondary nozzle's ($p_{o,s}$) inlet sections and the static pressure (p_d) at the outlet section of the ejector. No-slip conditions for the velocity and adiabatic boundary conditions are specified on the ejector wall. The flow turbulence is modeled using the SST $k-\omega$ equations with 5 percent turbulence intensity based on diameter of the secondary inlet, as it is well suited to predict ejector flow physics [Yann et al.(2006)]. A second-order upwind scheme is used for convective, viscous terms of the RANS equations, and for the turbulence transport equations. Iterative convergence is achieved when the scaled residual drops below 10^{-5} for the mean and turbulence variables.

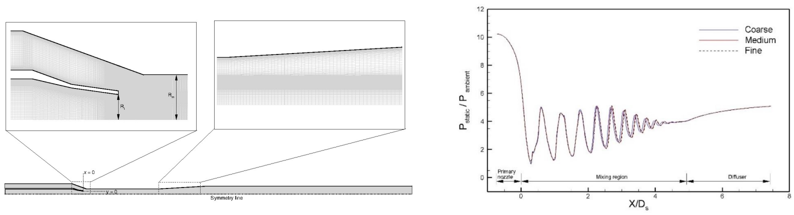

Figure 2: Grid structure of the computational domain for simulations (left). Pressure distribution along ejector axis for different mesh sizes. Length is non–dimensionalised by secondary nozzle inlet diameter, D$_s$ (right).

3 Results

Fig. 3 shows the entire operating map classified according to the primary flow or the combined/secondary flow. Analysing the ejector's flowfield at different operating conditions, the following regimes are identified:

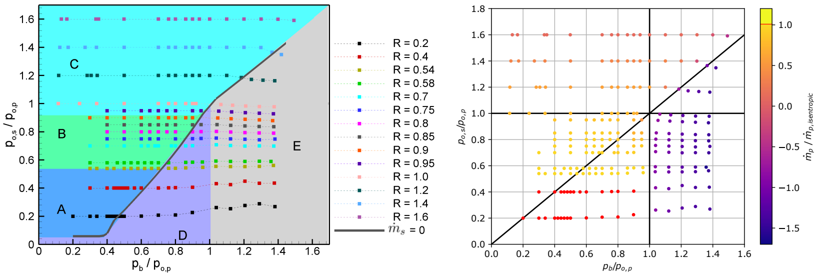

Figure 3: Operating Map (left) and Primary mass flow rate ($\dot{m}_p$) variation (right)

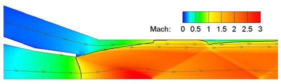

(a) Regime A: On-design

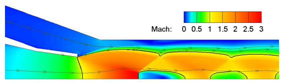

(b) Regime A: Off-design

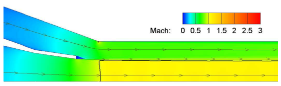

(c) Regime B

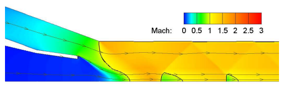

(d) Regime C

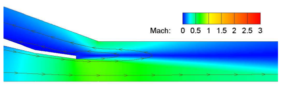

(e) Regime D

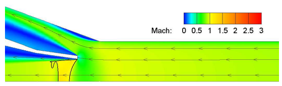

(f) Regime E

Figure 4: Mach number field exhibiting flow structure computed at different regimes. The stream- and sonic- lines are shown in grey and black colors, respectively.

- In regime A, the primary flow is sonic at the primary nozzle throat exhibiting both double choking (on-design, constant w) and single choking (off-design, decreasing w) modes depending on back pressure. At low back pressure, the flow in the mixing duct exhibits the Fabri flow pattern [Olivier (2017)], as shown in Fig. 4 a.

- In regime B, the primary flow is subsonic at the primary nozzle throat but becomes sonic further downstream (unchoked primary nozzle). This regime corresponds to the operating map with R ($p_{o,s}/p_{o,p}$) ranging in between 0.54 and 0.9.

- In regime C, the primary flow is subsonic at the primary nozzle throat and remains subsonic. The combined flow reaches Mach number (M) to one inside the mixing chamber after mixing (starting from the mixing chamber entry point) and because of the acceleration due to friction (Fanno choking). For $R >> 1$, the secondary stream accelerates isentropically to sonic velocities ($M_s > 1$) and the primary stream is entrained by the secondary flow, as shown in Fig. 4 d. Here, $\dot{m}_p + \dot{m}_s > 0$, normal flow at the secondary inlet $\dot{m}_s > 0$ and $w > 0$.

- In the regime D, the combined flow is unchoked with $\dot{m}_p + \dot{m}_s > 0$ but with reversed flow at the secondary inlet $\dot{m}_s < 0$ and $w < 0$. A limiting streamline line (grey line) leading from primary nozzle to the secondary nozzle (with $\dot{m}_s = 0$) clearly distinguish the normal mode to abnormal mode of operations.

- In regime E, the flow at the outlet is reversed with $\dot{m}_p < 0$ and $\dot{m}_s < 0$ (reversed flow at the inlet sections). For very high back pressure, the primary nozzle exhibits the reversed sonic primary flow (at the primary nozzle throat, as shown in Fig. 4 f).

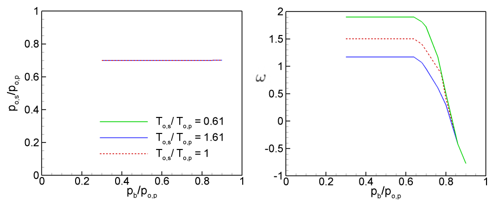

Figure 5: Temperature effect on ejector performance for $R = 0.7$.

Fig. 3 also shows the variation in the primary flow rate on the entire operating map. The maximum flow rate is represented by red dot, which corresponds to the choked flow in the primary nozzle. For $p_b/p_{o,p} < 1$, the flow inside the primary nozzle transitions from choked ($R < 0.54$) to unchoked ($R \geq 0.54$). In this regime, the total secondary pressure plays a key role in the choking condition of the primary flow. Along a characteristic line (fixed R), $\dot{m}_p$ is constant in the on-design mode; after that, $\dot{m}_p$ decreases in the off-design mode and reaches a minimum in the abnormal mode. Fig. 5 presents the temperature effect on the ejector's performance for $R = 0.7$ and the comparison is done for three temperature ratios of secondary total temperature to primary total temperature, i.e., $T_{o,s}/T_{o,p} = 0.61$, 1, and 1.61. Different values of $T_{o,p}$ and $T_{o,s}$ are considered for the analysis. For $T_{o,s} > T_{o,p}$, $\dot{m}_s$ decreases leading to the decrease in entrainment ratio in comparison with $T_{o,s} = T_{o,p}$ case. For $T_{o,s} < T_{o,p}$, the primary mass flow rate decreases and the entrainment increases in comparison with $T_{o,s} = T_{o,p}$ case. However, the entrainment ratio remains the same for the cases with $T_{o,s}/T_{o,p} = 1.61$ and 0.61, respectively. The cases with different R values show a similar temperature effect. Therefore, $T_{o,s}/T_{o,p}$ ratio or inlet total temperature plays a vital role on the ejector performance.

4 Conclusions

In this study, steady-state numerical computations are performed exploring the whole operating map for different $(p_b/p_{o,p}, p_{o,s}/p_{o,p})$ at a fixed $T_{o,s}/T_{o,p}$. The ejector's performance is distinguished depending on the operating conditions, such as total pressures and temperatures at primary/secondary inlets and outlet. All the operating conditions can be classified according to the primary flow and the combined flow regimes. These regimes allow us to characterize the ejector flow on the operating map completely. Thus, identifying the regimes on the whole operating range assists in developing an accurate and robust 0D model to model the ejector behavior. The inlet temperature strongly influences the mass flow rates, and the temperature ratio has thus an important impact on the entrainment ratio. However, the change in temperature ratio does not affect the pressure ratios and the flow regime types.

Acknowledgements

This project has received funding from the Clean Sky 2 Joint Undertaking (JU) under grant agreement No 101008100. The JU receives support from the European Union's Horizon 2020 research and innovation programme and the Clean Sky 2 JU members other than the Union.

Horizon 2020
European Union Funding
for Research & Innovation

Clean Sky 2

Disclaimer: The contents presented in this article reflect only the author's point of view: the authors and Clean Sky JU are not responsible for any use that may be made of the information it contains.

References

[Kulkarni et al.(2022)] Kulkarni, A., Yadav, S.K., and Kumar, A., "A comprehensive study on solar ejector cooling system: A review," *Materials Today: Proceedings*, pp. 2214-7853, (2022).

[Konstantinos (2021)] Konstantinos Braimakis, "Solar ejector cooling systems: A review," *Renewable Energy*, 164 pp. 566-602, (2021).

[Sagar et al.(2021)] Sagar, V., and Dibakar, R.,, "Recent advances and sustainable solutions in automobile air conditioning systems," *Journal of Cleaner Production*, 329 pp. 129754, (2021).

[Besagni et al.(2016)] Besagni, G., Mereu, R., and Inzoli, F., "Ejector refrigeration: A comprehensive review," *Renewable and Sustainable Energy Reviews*, 53 pp. 373-407, (2016).

[Qudama et al.(2022)] Qudama, A. Y., and Márta, S., and Müslüm, A.,, "A review on solar-powered cooling and air-conditioning systems for building applications," *Energy Reports*, 8, pp. 2888-2907, (2022).

[Yann et al.(2006)] Bartosiewicz, Y., AidounY, Z., and Mercadier, Y., "Numerical assessment of ejector operation for refrigeration applications based on CFD," *Applied Thermal Engineering*, 26 pp. 604-612, (2006).

[Vincent et al.(2012)] Lijo, V., Kim, H. S., Matsuo, S., Setoguchi, T., "A study of the supersonic ejector–diffuser system with an inlet orifice," *Aerospace Science and Technology*, 23 pp. 321-329, (2012).

[CleanSky2 (2021)] "Cordis. [Online]. Available: https://cordis.europa.eu/project/id/101008100"

[EUCASS (2022)] Schillaci, E., Oliet, Carles., Vemula, J. B., Duponcheel, M., Bartosiewicz. Y., and Planquart, P., "Air Ejector Analysis in Normal and Abnormal Modes, Oriented to Control Purposes in Aircraft Systems," 9^{th} *European Conference for Aeronautics and Space Science (EUCASS)*, (2022).

[Olivier (2017)] Lamberts, O., Chatelain, P., and Bartosiewicz. Y., "Numerical and experimental evidence of the Fabri-choking in a supersonic ejector," *International Journal of Heat and Fluid Flow*, 69 pp. 194-209, (2014).